Disruption of KCC2 Reveals an Essential Role of K-Cl Cotransport Already in Early Synaptic Inhibition

Christian A. Hübner,[1] Valentin Stein,[1]
Irm Hermans-Borgmeyer,[1] Torsten Meyer,[2]
Klaus Ballanyi,[2] and Thomas J. Jentsch[1,3]
[1] Zentrum für molekulare Neurobiologie Hamburg
ZMNH
Universität Hamburg
Martinistr. 52
D-20246 Hamburg
Germany
[2] Zentrum für Physiologie und Pathophysiologie
Universität Göttingen
Humboldtallee 23
D-37073 Göttingen
Germany

Summary

Synaptic inhibition by $GABA_A$ and glycine receptors, which are ligand-gated anion channels, depends on the electrochemical potential for chloride. Several potassium-chloride cotransporters can lower the intracellular chloride concentration $[Cl^-]_i$, including the neuronal isoform KCC2. We show that KCC2 knockout mice died immediately after birth due to severe motor deficits that also abolished respiration. Sciatic nerve recordings revealed abnormal spontaneous electrical activity and altered spinal cord responses to peripheral electrical stimuli. In the spinal cord of wild-type animals, the KCC2 protein was found at inhibitory synapses. Patch-clamp measurements of embryonic day 18.5 spinal cord motoneurons demonstrated an excitatory GABA and glycine action in the absence, but not in the presence, of KCC2, revealing a crucial role of KCC2 for synaptic inhibition.

Introduction

The function of the nervous system depends on an interplay between synaptic excitation and inhibition. In the adult mammalian central nervous system (CNS), GABA and glycine are the main inhibitory neurotransmitters, while glutamate is the main excitatory neurotransmitter. Ionotropic glutamate receptors are cation channels that have a high sodium conductance. Since physiological sodium gradients are directed inwardly, their opening always leads to an inward current and to a depolarization of the postsynaptic membrane that can be excitatory. GABA or glycine mediates synaptic inhibition by opening postsynaptic ligand-gated anion channels. The electrical response is governed by the electrochemical potential of the ions that are conducted by their pores. Depending on the particular cell, the intracellular chloride concentration can be below, at, or above equilibrium. Therefore, GABA and glycine can lead to a hyperpolarization, an increase in membrane conductance without changing the voltage, or a depolarization of the

cell. The first two situations result in synaptic inhibition, while a depolarization that reaches the threshold of action potential generation can be excitatory. Changing the intracellular Cl^- concentration $([Cl^-]_i)$ therefore provides a means to regulate the response to GABA or glycine.

In fetal life and early postnatal development, both neurotransmitters act mostly excitatory because the intracellular chloride concentration is above equilibrium. The excitatory action of GABA in the immature CNS is believed to be important for the development of the nervous system, as it may exert a trophic action through membrane depolarization and an ensuing rise in intracellular Ca^{2+} (Cherubini et al., 1991; LoTurco et al., 1995; Yuste and Katz, 1991). Since glutamatergic synaptic transmission is first purely NMDA receptor based, the depolarization by GABA may be necessary to provide the initial depolarization that is needed to relieve the voltage-dependent Mg^{2+} block of NMDA receptors (Ben-Ari et al., 1997). During the maturation of the CNS, there is a widespread decrease of neuronal $[Cl^-]_i$, which is finally below its equilibrium, so that the opening of the $GABA_A$ or the glycine receptor leads to an inflow of Cl^- and an inhibitory hyperpolarization of the cell. The most important players are probably members of the cation-chloride cotransporter gene family. This family includes the Na-Cl cotransporter (NCC), the Na-K-2Cl cotransporters (NKCC), which typically raise $[Cl^-]_i$, and K-Cl cotransporters (KCCs), which normally lower $[Cl^-]_i$ below its electrochemical equilibrium potential. Consistent with their differential tissue distributions, their function is not restricted to regulate neuronal $[Cl^-]_i$. Several of these transporters play important roles in transepithelial transport and cell volume regulation. These functions are demonstrated by diseases that result from mutations in their genes. Mutations in *NCC* and *NKCC2* underlie Gitelman's syndrome (Simon et al., 1996b) or a form of Bartter's syndrome (Simon et al., 1996a), respectively, tubulopathies that are associated with massive renal salt loss. Disruption of *NKCC1* in mice leads to a severe degeneration of the inner ear (Delpire et al., 1999) and to male infertility (Pace et al., 2000), phenotypes that can be attributed to defects in transepithelial transport as well. Although *NKCC1* is also expressed in neurons, where it presumably raises $[Cl^-]_i$ already early in development, no major neuronal phenotype of NKCC1-deficient mice has been reported though the GABA response of isolated dorsal root ganglion cells was shifted (Sung et al., 2000).

The *KCC* gene family comprises four members (Mount et al., 1999). Among these, KCC2 is a neuronal isoform that is broadly expressed in the adult CNS (Payne et al., 1996). Depending on the chemical concentration gradients of potassium and chloride, this transporter can operate as a net efflux or influx pathway, which further implies the movement of water. It is becoming clear that this transporter plays a significant role in dynamic changes of ion concentrations and water during synaptic transmission (Voipio and Kaila, 2000). In the rat hippocampus, the incipient expression of KCC2 correlates
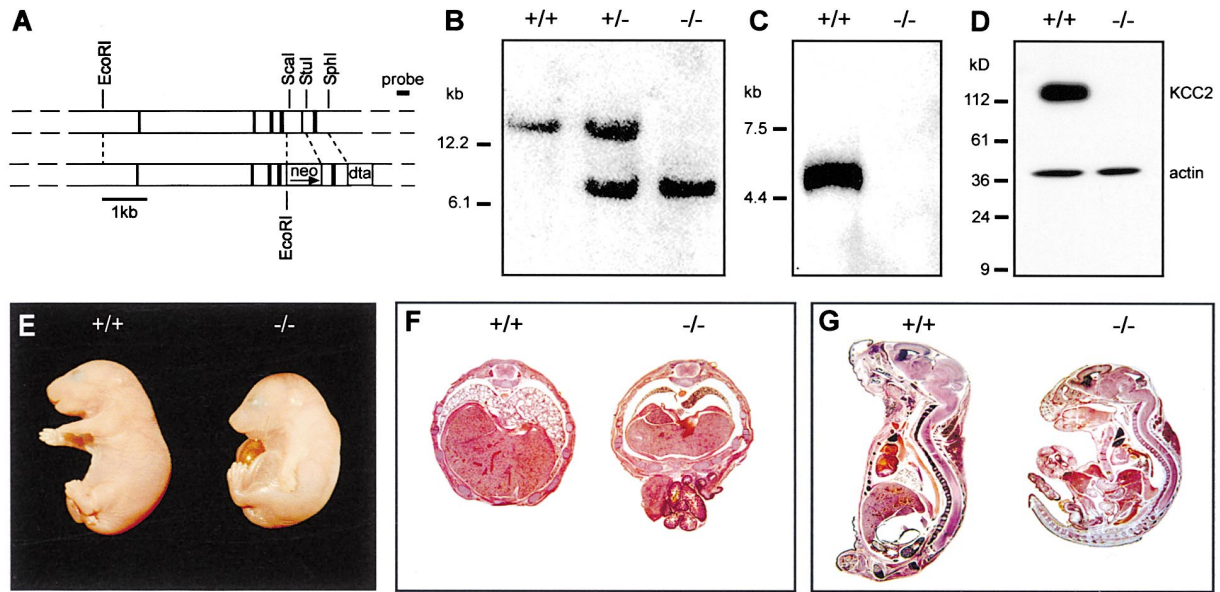
[3] Correspondence: jentsch@zmnh.uni-hamburg.de

Figure 1. Targeted Disruption of *Kcc2* and Its Effect on Mice

(A) The WT *Kcc2* gene and the targeted allele, exons symbolized as black bars. Exon 5 was replaced by a neomycin selection cassette (neo). A diphtheria toxin A subunit cassette (dta) was introduced as a negative selection marker.

(B) Southern blot analysis with the 3′ probe shown in (A) exploited an additional EcoRI site and resulted in a smaller band for the targeted gene.

(C) Northern blot analysis of brain poly(A)$^+$ RNA with a probe spanning exon 5 shows that WT KCC2 transcripts are absent in mutant mice.

(D) In Western blot analysis of brain lysates, an amino-terminal KCC2 antibody detected the expected ≈140 kDa KCC2 band in WT mice. It was absent in *Kcc2*$^{-/-}$ animals. An actin antibody was used as a loading control.

(E) Compared to a WT littermate (left), the mutant animal (right) did not move and breathe spontaneously. Forelimbs were maximally extended. *Kcc2*$^{-/-}$ animals often had omphaloceles. Weights of *Kcc2*$^{-/-}$ and *Kcc2*$^{+/+}$ animals did not differ significantly.

The corresponding horizontal (F) and sagittal midline (G) sections revealed severe atelectasis of the lungs in *Kcc2*$^{-/-}$ animals (HE staining). No gross defects of the central nervous or the musculo-skeletal system were detectable.

with the switch from a depolarizing to a hyperpolarizing action of GABA that occurs around postnatal day 9 (P9) (Rivera et al., 1999). The suggestion that KCC2 is the dominating neuronal Cl$^-$ extrusion mechanism was supported by antisense experiments in vitro (Rivera et al., 1999). Therefore, KCC2 knockout (KO, *Kcc2*$^{-/-}$) mice were expected to develop neurological defects after birth. Unexpectedly, *Kcc2*$^{-/-}$ animals had severe motor deficits already at birth and died due to a failure of respiration. Sciatic nerve reflexes were abnormal and motoneurons showed an excitatory response to GABA or glycine that contrasted with an inhibitory response seen in wild-type (WT) mice of the same age. This shows that the functional GABA/glycine switch in the spinal cord occurs earlier than in the hippocampus. It depends crucially on the expression of KCC2, and is indispensable for the normal function of motor circuits already at birth.

Results

Kcc2$^{-/-}$ Mice Die Immediately after Birth due to Hypoxia

To investigate the physiological role of KCC2, we disrupted its gene in mice. Deletion of the fifth exon of the *Kcc2* gene (Figure 1A), which codes for the first half of the second putative transmembrane domain, caused a frameshift and thereby truncated the protein in exon 6.

Targeted embryonic stem (ES) cell clones were identified by Southern blot analysis, which exploited a newly introduced EcoRI site. With a 3′ probe, an ∼8 kb smaller fragment was detected for the mutant allele (Figure 1B). Two independent correctly targeted embryonic stem (ES) cell clones were injected into blastocysts and gave heterozygous offspring. Heterozygous animals had no obvious phenotype: life expectancy and simple behavioral tests, as well as the response to seizure-inducing agents (Prichard et al., 1969), were not different from WT mice (*Kcc2*$^{+/+}$) (data not shown). Homozygous mutants (*Kcc2*$^{-/-}$) developed in utero at the expected Mendelian ratio (32 *Kcc2*$^{-/-}$ out of 127 littermates) but died within 15 min after birth. We therefore sacrificed pregnant mice before spontaneous delivery at day 18.5 of gestation to recover the offspring via Cesarean section. Heterozygous and WT embryos consistently survived this procedure. The absence of the WT KCC2 transcript and protein in *Kcc2*$^{-/-}$ animals was confirmed by Northern (Figure 1C) and Western blot analysis (Figure 1D). Because the antibody was directed against an amino-terminal epitope, the Western analysis also revealed the virtual absence of a truncated protein (expected size ∼18 kDa) that might be expressed from the construct. *Kcc2*$^{-/-}$ animals were characterized by an abnormal flexor-extensor posturing (Figure 1E), indicating a severe motor deficit. They did not move spontaneously and reacted only to strong mechanical stimuli. All *Kcc2*$^{-/-}$
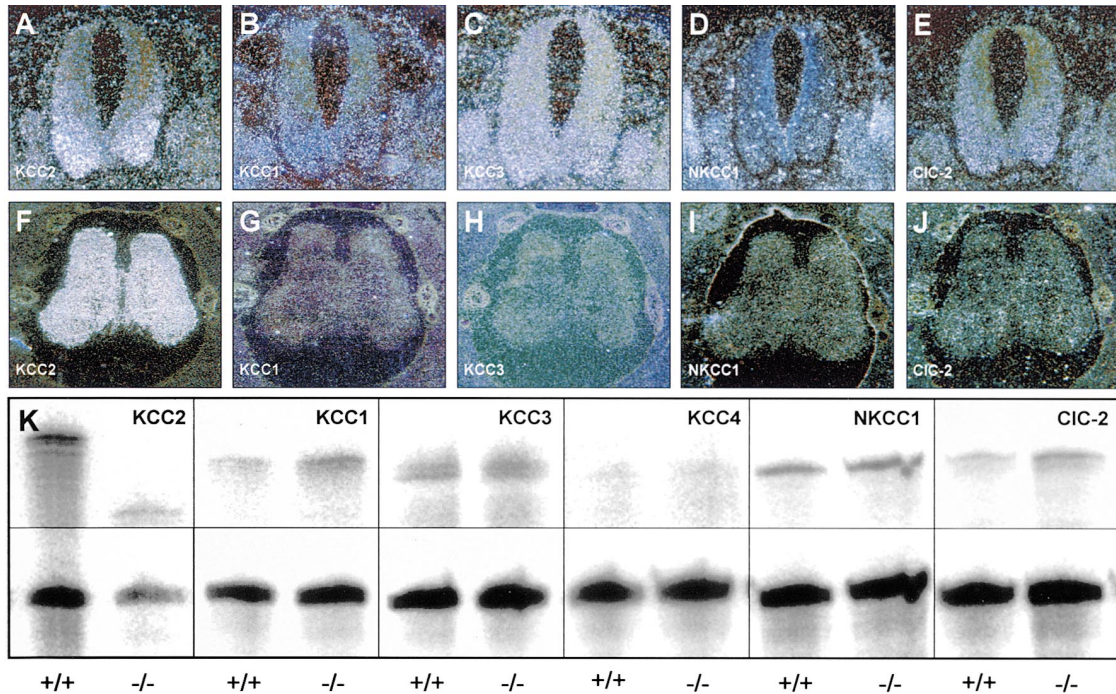
Figure 2. mRNA Expression of Various Cl⁻-Transporting Proteins in the Developing Spinal Cord

Darkfield photomicrographs of adjacent transverse sections subjected to in situ hybridization are shown (A–J). Signals appear as white grains. At E12.5 (A–E), the KCC2 transcripts accumulated in the ventral horns (A). Signals for KCC1 (B), KCC3 (C), NKCC1 (D), and ClC-2 (E) transcripts were less pronounced in the spinal cord, but were also seen in spinal ganglia, which flank the spinal cord on both sides. Signals for NKCC1 were concentrated at single scattered cells. At E18.5 (F–J), KCC2 signals were more prominent. With the exception of KCC2, transcripts were not restricted to neurons. (K) Expression of KCC1, KCC2, KCC3, KCC4, NKCC1, and ClC-2 transcripts in the spinal cord of E18.5 $KCC2^{+/+}$ and $KCC2^{-/-}$ littermates was investigated by ribonuclease protection assays. The KCC2 probe spanning exon 5 of $Kcc2$ was degraded to a shorter fragment in the mutant. When normalized to actin (lower panel), the $KCC2^{-/-}/KCC2^{+/+}$ ratios of transcripts were: KCC1 (134% ± 18%), KCC3 (96% ± 9%), KCC4 (117% ± 15%), NKCC1 (97% ± 13%), and ClC-2 (103% ± 6%) (n = 3, ± SEM). Differences between KO and WT were not significant.

animals failed to breathe and had lung atelectasis (Figures 1F and 1G). $Kcc2^{-/-}$ lungs sunk whereas control lungs floated on water. $Kcc2^{-/-}$ mice had abdominal wall defects ranging from an increased abdominal prominence to omphaloceles without any obvious histological abnormalities. A defect of the diaphragm was excluded by injecting dye into the thoracic cavity. Apart from the lung atelectasis, we could not detect any gross histological defects in $Kcc2^{-/-}$ animals. Spinal cord and brainstem nuclei of $Kcc2^{-/-}$ animals did not differ morphologically from control littermates (data not shown). This included the medullary respiratory center localized in the pre-Bötzinger complex (Smith et al., 1991).

To exclude heart failure as the primary cause of the neonatal death of $Kcc2^{-/-}$ animals, we recorded electrocardiograms (ECG) of $Kcc2^{-/-}$ and WT animals. However, heart rate and amplitude were identical immediately after birth and only gradually declined due to hypoxia (data not shown). According to these data, we speculated that $Kcc2^{-/-}$ animals have severe motor deficits and die due to an inability to breathe.

KCC2 Expression Starts during Motoneuron Differentiation

To gain an impression of the contribution of KCC2 to the regulation of [Cl⁻]ᵢ in the developing spinal cord, we compared its expression to those of other chloride-

transporting proteins. KCC1 is the housekeeping isoform of the KCC transporter family and is almost ubiquitously expressed (Gillen et al., 1996). By Northern analysis, KCC3 showed a more restricted expression pattern, which included the adult CNS (Mount et al., 1999). As NKCC2 (Haas and Forbush, 1998) and KCC4 (Mount et al., 1999) are not significantly expressed in the brain, we rather included the voltage-gated Cl⁻ channel ClC-2 (Thiemann et al., 1992), which is thought to modify the GABA response in certain neurons (Staley et al., 1996). At embryonic day 12.5 (E12.5), strong signals for KCC2 transcripts were detected in the ventral horns of the spinal cord (Figure 2A), where motoneurons are located (Wentworth, 1984), but were absent in spinal ganglia. KCC1, KCC3, and ClC-2 transcripts were expressed more diffusely in the spinal cord and in spinal ganglia (Figures 2B, 2C, and 2E) as well as in other tissues (data not shown). NKCC1 transcripts were detected in some cells of the spinal cord and in spinal ganglia (Figure 2D). Around birth (E18.5), KCC2 transcripts were detectable throughout the spinal cord (Figure 2F) along the complete neuraxis including the medulla with the pre-Bötzinger complex. In contrast, the spinal cord signals for the other transporters and ClC-2 had decreased when compared to E12.5 (Figures 2G–2J). To test whether the expression of the other transporters is affected by the disruption of $Kcc2$, RNA was prepared of E18.5 spinal
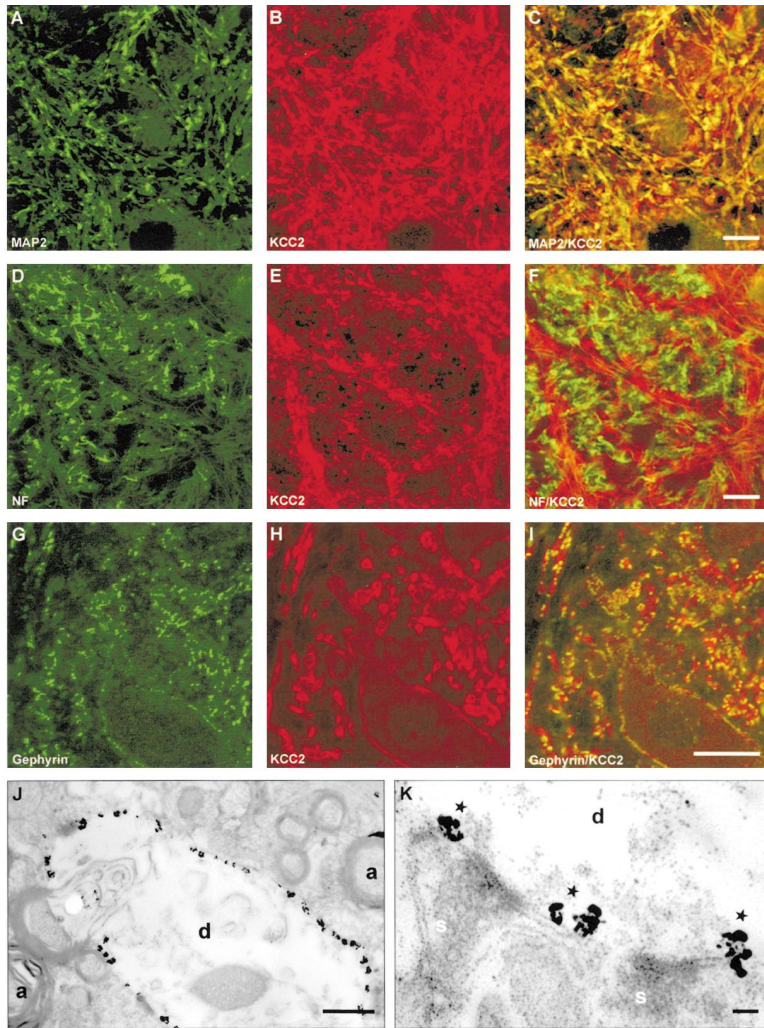
Figure 3. Expression of the KCC2 Protein in the Spinal Cord

Ventral horn motoneurons embedded into a network of axons and dendrites projecting into the white matter of the spinal cord are shown (A–I). Immunofluorescence demonstrated that KCC2 (red) is coexpressed with the dendritic marker MAP2 (green) (A–C), but not with NF (green) (D–F) at E18.5. Overlapping expression appears as yellow. KCC2 also colocalized with gephyrin (green) (G–I) in adult spinal cord. (J) Electron microscopy on WT adult spinal cord confirms accumulation of KCC2 along the plasma membrane of dendrites (d) but not in axons (a). (K) The ultrastructure of a spinal cord dendrite (d) revealed that immunogold-labeled KCC2 (asterisks) is located in proximity to synapses (s). The bars represent 10 μm, except for (J) (1 μm) and (K) (100 nm).

cords of both genotypes and subjected to ribonuclease protection assays. We normalized the intensities to the corresponding actin band and calculated the relative expression between $Kcc2^{-/-}$ and WT animals. Transcripts for KCC2 were shortened in $Kcc2^{-/-}$ mice due to the loss of exon 5. Transcripts for KCC1, KCC3, KCC4, NKCC1, and ClC-2 were not significantly changed in $Kcc2^{-/-}$ mice (Figure 2K). These data were confirmed qualitatively by in situ hybridization of $Kcc2^{-/-}$ sections with the same probes used for in situ hybridization of WT sections (data not shown).

KCC2 Is Localized at Inhibitory Synapses

The KCC2 antiserum was raised in rabbits against an amino-terminal epitope and affinity purified. It was highly specific, as no signals were detected in $Kcc2^{-/-}$ mice by Western analysis (Figure 1D) or immunofluorescence (data not shown). To investigate the subcellular localization of the KCC2 protein in the mouse spinal cord at E18.5, we costained sections for KCC2 and for the dendritic marker microtubule-associated protein 2 (MAP2) or the axonal marker neurofilament-associated antigen (NF). KCC2 colocalized with MAP2 (Figures 3A–3C), but not with NF (Figures 3D–3F), indicating that

KCC2 is mainly expressed in dendrites of spinal cord neurons. KCC2 also widely colocalized with gephyrin in the adult spinal cord (Figures 3G–3I), a postsynaptic protein involved in the clustering of glycine and GABA$_A$ receptors (Kneussel and Betz, 2000). While sites stained for gephyrin nearly always costained for KCC2, only $\sim$70% of the KCC2 signals colocalized with gephyrin. Thus, KCC2 is predominantly, but not exclusively, localized at gephyrin-positive inhibitory synapses. Electron micrographs of KCC2/immunogold stained spinal cord sections confirmed the expression of KCC2 in the plasma membrane of dendrites and its absence in axons in the adult spinal cord (Figure 3J). These were distinguished from dendrites by their myelinization and their neurofilament skeleton. KCC2 was expressed at synapses (Figure 3K). It was enriched at the periphery of the postsynaptic specialization, whereas gephyrin is known to form a postsynaptic matrix that coextends with the active zone. In summary, KCC2 is localized at inhibitory synapses of the spinal cord.

$Kcc2^{-/-}$ Mice Show Abnormal Motoneuron Activity

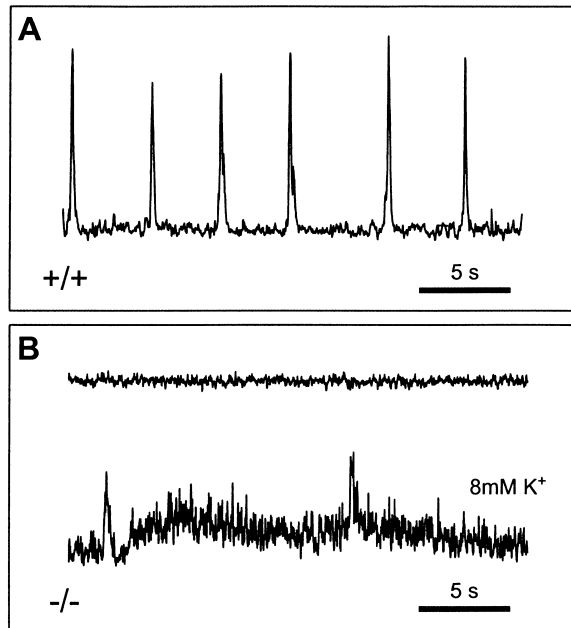The localization of KCC2 at inhibitory synapses is compatible with a role of KCC2 in the modulation of moto-

Figure 4. Respiratory Motor Output of Isolated Brainstem Preparations of E18.5 Mice

(A) Preparations from control animals (n = 5) had spontaneous rhythmic activity, which was absent in $Kcc2^{-/-}$ brainstem preparations (n = 5) (B, upper trace). In $Kcc2^{-/-}$ mice, irregular slow rhythmic activity was only seen after raising extracellular K^+ to 8 mM (B, lower trace), thereby confirming the vitality of the preparation. Recordings were obtained over periods of >120 min for each preparation. Traces show filtered and integrated activity.

neuron responses to GABA and glycine. As motoneurons provide the drive to respiratory muscles and $Kcc2^{-/-}$ animals did not breathe, we monitored the inspiratory-related motor output of the pre-Bötzinger complex from cervical ventral rootlets of isolated brainstem preparations (Suzue, 1984). Preparations from control animals had a normal, regular rhythm of roughly 14 electrical bursts per minute (Figure 4A), which was stable for several hours during superfusion with oxygenated artificial cerebrospinal fluid at 30°C (n = 5). In contrast, preparations from $Kcc2^{-/-}$ animals were not rhythmically active (Figure 4B, upper trace) and a regular rhythm could neither be induced by application of the $GABA_A$ receptor blocker bicuculline nor by the glycine receptor blocker strychnine, nor by a combination of both antagonists (data not shown) (n = 5). However, raising the extracellular potassium concentration to 8 mM established irregular respiratory activity of $Kcc2^{-/-}$ brainstems (Figure 4B, lower trace). This confirmed the vitality of the preparations.

Given the abnormal posture of mutant mice, we monitored the electrical activity of the sciatic nerve in mutant and control animals. The sciatic nerve includes afferent fibers, e.g., from muscle spindles, and efferent fibers innervating muscles of the hindlimb (Figure 5A). Numerous bursts and spontaneous motoneuron action potentials were consistently recorded in $Kcc2^{-/-}$ animals (roughly 30 spikes/min; n = 5), whereas spontaneous activity was rare in all control preparations and was never sustained (roughly 4 spikes/min; n = 5). As a

quantitative measure of burst activity, we determined the probability of observing a spike within 5 s of a preceding spike. It was 98% in the KO, but 0% in WT. Similar bursting activity could be evoked in the WT by the application of bicuculline and strychnine (n = 3) (Figure 5B).

We then tested the spinal cord responses to the electrical stimulation of the sciatic nerve in animals of both genotypes (Buckle and Spence, 1981). The threshold of sciatic nerve preparations was approximately 10 V irrespective of the genotype. The spinal cord response to threshold stimuli was polyphasic in all tested mutant animals and its pattern varied from stimulus to stimulus, contrasting with the stereotypic biphasic responses in control experiments with wild-type preparations. Application of strychnine and bicuculline in WT preparations resulted in similar responses as in $Kcc2^{-/-}$ mice preparations (n = 3) (Figure 5C). These data show that the disruption of KCC2 interferes with the function of α motoneurons.

GABA and Glycine Are Excitatory for $Kcc2^{-/-}$ but Not on WT Motoneurons

To analyze motoneuron membrane potentials without disturbing $[Cl^-]_i$, we used a gramicidin perforated patch-clamp technique (Kyrozis and Reichling, 1995). Recordings were obtained from motoneurons that were located in the ventral part of E18.5 spinal cord slices. If not otherwise indicated, tetrodotoxin (TTX, 500 nM) was added to the superfusate to exclude network effects during agonist application. The resting potential was not altered in $Kcc2^{-/-}$ motoneurons (−66.8 ± 5.6 mV (SEM; n = 8) for $Kcc2^{-/-}$; −64.6 ± 2.0 mV (SEM; n = 8) for WT). Upon GABA or glycine application (100 μM), neurons of $Kcc2^{-/-}$ animals depolarized to −35.3 ± 5.1 mV (n = 5) and to −36.9 ± 7.2 mV (n = 3), respectively. In control animals, the neurons depolarized only to −56.4 ± 3.2 mV (n = 5) with GABA and to −54.3 ± 4 mV (n = 3) with glycine (± SEM). ΔV for both genotypes is shown in Figure 6A. The voltage response could be blocked by bicuculline and strychnine in both genotypes (data not shown). The voltage obtained upon agonist application provides an estimate of the Cl^- equilibrium potential under the assumption that the agonist-induced currents were dominant and that they were not significantly carried by HCO_3^-. This suggests that the loss of KCC2 led to a significant increase of $[Cl^-]_i$ in E18.5 motoneurons. The GABA-induced shift of the reversal potential was also determined under voltage-clamp conditions (Figures 6B and 6C): in $Kcc2^{-/-}$ motoneurons, the reversal potential shifted from −64.6 ± 4.2 mV to −33.1 ± 6.4 mV (n = 5), whereas in WT, it was changed from −63.5 ± 3.4 mV to −52.2 ± 5.2 mV (n = 5). This agrees very well with the current clamp experiments.

The absence of action potentials during GABA application in TTX free recordings of E18.5 WT motoneurons (Figure 6D) demonstrated that GABA had already an inhibitory effect. In $Kcc2^{-/-}$ motoneurons, however, the depolarization induced by GABA or glycine was strong enough to cause multiple action potentials, revealing an excitatory action of both neurotransmitters (Figure 6E), which was not observed in WT motoneurons.
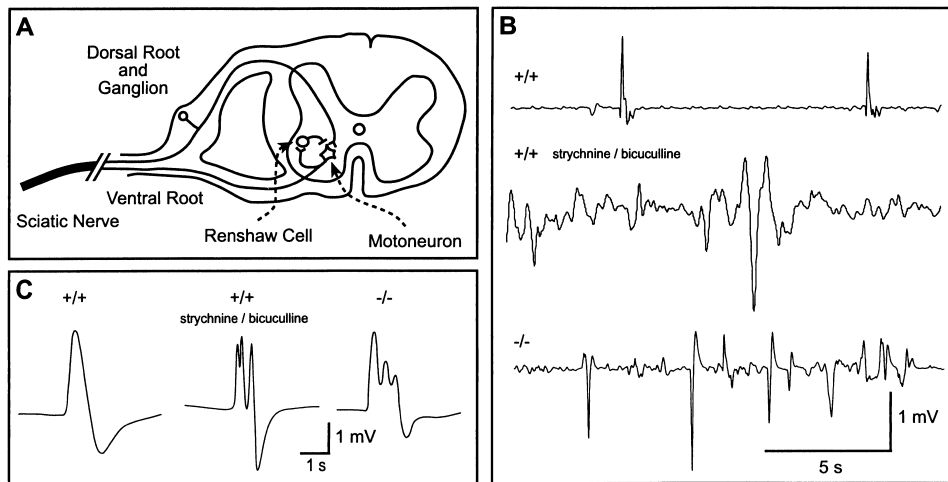
Figure 5. Recordings of Spinal Cord Responses to Peripheral Stimuli

(A) Simplified scheme of a spinal cord segment showing the components of the monosynaptic reflex. GABA and glycinergic spinal cord interneurons are activated via axon collaterals. Afferent and efferent fibers form the sciatic nerve.

(B) In sciatic nerve recordings of WT animals, rare spontaneous action potentials have been observed (five independent preparations). However, bursts of spontaneous activity were absent. All preparations obtained from $Kcc2^{-/-}$ animals (n = 5) had bursts of spontaneous activity, interrupted by periods with no activity. Preparations from control animals superfused with ASCF containing 250 μM strychnine and 250 μM bicuculline (n = 3) showed a similar pattern of spontaneous activity as $Kcc2^{-/-}$ preparations. Registrations periods were always >15 min.

(C) Upon electrical stimulation of the sciatic nerve, a biphasic response was seen in control animals (n = 5). Polymorphic spinal cord responses were recorded in mutant preparations (n = 5) and in WT preparations after application of bicuculline and strychnine (250 μM each) (n = 3). Reflex measurements were repeated >20 times for each preparation.

Discussion

The response of GABA$_A$ and glycine receptors, which are postsynaptic ligand-gated anion channels, depends on the electrochemical potential for chloride. Low intracellular chloride leads to an inhibitory response to GABA or glycine, while high chloride can cause an excitatory response, which is thought to be essential for the consolidation of synaptic connections and the maturation of the neuronal network and may be due to an influx of Ca^{2+} via voltage-dependent Ca^{2+} channels or NMDA receptor channels (Cherubini et al., 1991; Flint et al., 1998; Goodman and Shatz, 1993; LoTurco et al., 1995; Obrietan and van den Pol, 1997; Yuste and Katz, 1991). Therefore, disturbing the physiological reversal of the response to GABA or glycine by disrupting KCC2 might interfere with the structural maturation of the CNS. However, apart from lung atelectasis, we did not observe any obvious histological changes in neonatal $Kcc2^{-/-}$ mice including the spinal cord and brain.

We investigated the chain of events that leads from the disruption of the K-Cl cotransporter to the macroscopic phenotype by focusing on motoneurons, whose circuitry is relatively well understood. In addition to KCC2, several other transporters may influence $[Cl^-]_i$ of motoneurons to yield an inhibitory GABA response. For example, the voltage-gated chloride channel ClC-2 (Thiemann et al., 1992) is thought to keep $[Cl^-]_i$ close to its electrochemical equilibrium in certain neurons, an effect predicted to lead to an inhibitory GABA response (Smith et al., 1995; Staley et al., 1996). In contrast to the present knockout, however, mice lacking the ClC-2 channel are viable and show no overt signs of neuronal hyperexcitability (Bösl et al., 2001). To estimate the con-

tribution of several transport mechanisms to Cl$^-$ homeostasis in motoneurons, we compared the expression of KCC1, KCC2, KCC3, NKCC1, and ClC-2 in the developing mouse spinal cord. KCC2 expression started very early, different from the phylogenetically younger parts of the neuraxis (Clayton et al., 1998). Spinal cord motoneurons were labeled for KCC2 as early as E12.5. KCC2 expression spread over the complete spinal cord at E18.5, whereas spinal ganglia remained unlabeled. Other members of the K-Cl cotransporter family and ClC-2 were expressed early (at E12.5), but hybridization signals were weaker in the spinal cord at E18.5.

By contrast to the transporters discussed above, NKCC1 normally raises $[Cl^-]_i$ above its electrochemical equilibrium and could therefore oppose the action of the KCCs. In vitro experiments suggested that a loop diuretic-sensitive cotransport such as NKCC1 may be responsible for the Cl$^-$ accumulation into neurons that underlies an excitatory GABA response (Sun and Murali, 1999). The probe for NKCC1 transcripts spanned part of exon 1 and exons 2 to 4 so that transcripts of an alternative splice variant, which was previously shown to be primarily expressed in the brain, were also detected (Randall et al., 1997). In E12.5 spinal cord, NKCC1 transcripts appeared to be concentrated in single scattered cells. This pattern had almost disappeared at E18.5. Hence, NKCC1 may not be the major transporter leading to an excitatory GABA response in the embryonic spinal cord and may not be able to compensate functionally the early expression of KCC2.

Consistent with its proposed role in synaptic inhibition of motoneurons, the KCC2 protein was present along dendrites and the plasma membrane of motoneuron somata of the E18.5 spinal cord. At the light-microscopic
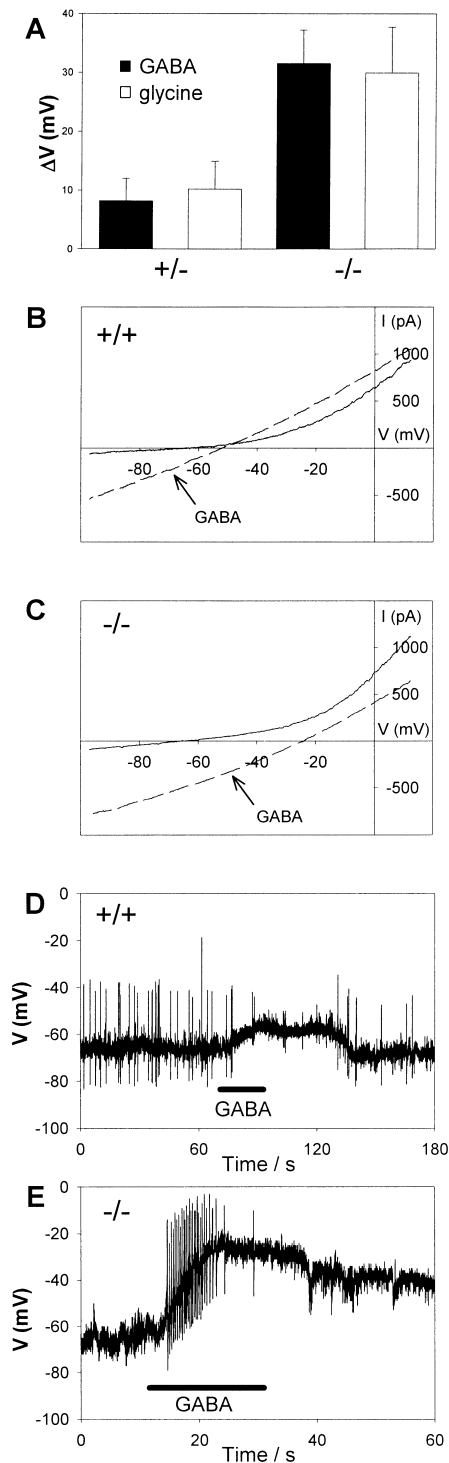
Figure 6. Electrophysiological Studies on Spinal Cord Motoneurons

Using gramicidin perforated patches, membrane potentials were recorded in the current-clamp (I = 0) mode (A,D, and E) or currents in the voltage-clamp mode (B and C). (A) Neurons of either genotype depolarized upon application of 100 μM GABA or 100 μM glycine for 30 s, but the depolarization was significantly increased in $Kcc2^{-/-}$ animals. The mean resting potential was -66.8 ± 5.6 mV (SEM; n = 8) in $Kcc2^{-/-}$ animals and -64.6 ± 2.0 mV (SEM; n = 8) in control animals. In $Kcc2^{-/-}$ animals, motoneurons strongly depolarized upon applying GABA ($\Delta V = 31.5 \pm 5.7$ mV; n = 8) or glycine ($\Delta V = $

level, gephyrin, a protein that anchors and immobilizes glycine receptors on the subsynaptic skeleton (Kirsch and Betz, 1995), was almost always colocalized with KCC2. However, KCC2 staining was also found in regions where gephyrin was not detected (Figure 3I). Electron microscopy confirmed that KCC2 was expressed at synapses, where it was concentrated at sites directly flanking synaptic clefts. This localization might be needed to maintain local postsynaptic chloride gradients during the opening of ligand-gated anion channels. In other brain regions too, KCC2 was mainly expressed in dendrites and colocalized with ligand-gated anion channels as shown recently for the adult rat cerebellum (Williams et al., 1999). KCC2 expression has also been shown at sites of GABAergic inhibition in the retina (Vardi et al., 2000; Vu et al., 2000). Thus, morphological data fit well with the proposed role of KCC2 as an important Cl^- extrusion mechanism in neurons. Indeed, we were able to demonstrate indirectly an altered $[Cl^-]_i$ in $Kcc2^{-/-}$ motoneurons. The depolarization amplitude after application of GABA or glycine, respectively, was significantly larger in $Kcc2^{-/-}$ than in WT animals. As a consequence, GABA-induced depolarization elicited multiple action potentials in KO motoneurons. In contrast, though GABA- and glycine-activated Cl^- efflux also moderately depolarized WT motoneurons, it reduced their excitability. This may be due to the increased conductance which can shunt excitatory synaptic currents (Gao and Ziskind-Conhaim, 1995), or may be caused by a voltage-dependent inactivation of Na^+ channels (Zhang and Jackson, 1993).

These findings prompted us to test spinal cord reflexes in WT versus $Kcc2^{-/-}$ preparations. We chose the anatomically well-defined sciatic nerve, which includes afferent fibers from proprioceptive receptors and efferent fibers that innervate various muscles of the hindlimb. By electrical stimulation, it is possible to preferentially activate group Ia afferents that originate from muscle spindles because they have lower thresholds than the efferent axons of α motoneurons (Lloyd, 1943). Hence, we could test the monosynaptic reflex by stimulating and recording the same nerve. This reflex involves muscle spindles afferents, which project to the correspond-

29.9 $\pm$ 7.8 mV; n = 4). WT animals responded with significantly lower depolarizations to GABA ($\Delta V = 8.2$ mV $\pm$ 3.7; n = 5) and glycine ($\Delta V = 10.3 \pm 4.7$ mV; n = 3) and sometimes even hyperpolarized. (B) shows the I/V relationship for WT, (C) for $KCC2^{-/-}$ motoneurons in the absence and presence of GABA. Under voltage-clamp conditions, a comparable depolarization was observed as in the current-clamp mode: $\Delta V = 11.5 \pm 6.2$ mV; n = 5 (WT); $\Delta V = 31.5 \pm 7.6$ mV; n = 5 ($Kcc2^{-/-}$). ([B] and [C] show representative individual recordings.) These experiments were performed in the presence of tetrodotoxin to abolish network effects. (D) GABA inhibited action potentials in control motoneurons, whereas action potentials were elicited by the GABA-induced depolarization in mutant animals (E). The use of perforated patch measurements entails a relatively high access resistance that leads to biphasic shapes of action potentials, but does not affect the measurement of the much slower depolarization. ([D] and [E] show individual recordings representative of five independent experiments done in the absence of tetrodotoxin. There was no systematic difference in spontaneous activity between WT and KO. Spontaneously active and inactive neurons were chosen for WT and KO genotypes, respectively, to show the opposite effects of GABA.)

ing α motoneurons. The stimulus threshold as well as the response latency did not differ between genotypes, indicating that the integrity of the sciatic nerve was not affected. However, the spinal cord response of $Kcc2^{-/-}$ mice was polyphasic and varied in duration, contrasting with the stereotypic biphasic response in WT animals. This response resembles the reflex pattern obtained from the *spastic* mouse mutant (Biscoe and Duchen, 1986), which carries a mutation in the glycine receptor, and our WT reflex pattern after application of bicuculline and strychnine. These observations significantly strengthen the conclusion that KCC2 is crucial for synaptic inhibition. The polyphasic response of $Kcc2^{-/-}$ spinal cords can be explained by the superimposition of asynchronous compound action potentials due to the loss of GABA- and glycinergic-inhibitory control of α motoneurons. Various interneurons are involved in the tuning of the α motoneuron response to external stimuli. These include Renshaw cells, which are reciprocally activated by α motoneuron collaterals and project to motoneurons via GABAergic and glycinergic transmission (Schneider and Fyffe, 1992).

The spontaneous electrical sciatic nerve activity should reflect the resting muscle tone of the hindlimb. $Kcc2^{-/-}$ mice had a drastically increased spontaneous sciatic nerve activity compared to their WT littermates, indicating a spastic disorder. An overall increased muscle tone probably explains the abnormal curved posture of the trunk and the maximally extended forelegs. The spontaneous sciatic nerve hyperactivity contrasted with the absence of spontaneous activity of brainstem cervical rootlets, indicating a different mechanism of control in rostral parts of the spinal cord. Registrations of ventral cervical rootlet activity do not give clues as to whether this is caused by a primary defect in the rhythmogenic brainstem center or by a failure to transmit this activity to motoneurons. Respiratory rhythmogenesis itself depends on a small group of excitatory and inhibitory neurons located in the pre-Bötzinger complex of the medulla (Smith et al., 1991) and is a complex phenomenon involving multiple excitatory and inhibitory interactions that are not yet fully understood. Cl⁻-dependent inhibition is critical in burst pattern formation, but is not necessary for rhythm generation itself (Ballanyi et al., 1999; Feldman and Smith, 1989). Hence, suffocation of $Kcc2^{-/-}$ mice may rather be caused by a defect in the transmission of the respiratory drive from the rhythmogenic pre-Bötzinger complex interneurons to the respiratory motoneurons.

In summary, we have shown that KCC2 establishes postsynaptic chloride gradients that are important for synaptic inhibition by GABA or glycine. KCC2 plays a pivotal role already in the neonate brainstem and the spinal cord, where it is essential for normal motoneuron function and spinal cord reflexes. As a consequence, its disruption leads to an abnormal muscle tone, defects in motor control, and to an inability to breathe, which results in perinatal death.

Experimental Procedures

Targeted Disruption of *Kcc2*

A clone isolated from a 129/SvJ mouse genomic λ library (Stratagene) was used to construct a targeting vector. A 8.5 kb EcoRI/

ScaI fragment including exons 1 to 4 and a 1.7 kb StuI/SspI fragment including exon 6 were placed in the Scrambler V901 vector (Lexicon Genetics), flanking a phosphoglycerate kinase (pgk) promoter-driven neomycin resistance cassette. A pgk promoter-driven diphtheria toxin A cassette was added as a negative selection marker. The construct was electroporated into RW4 ES cells. Resistant clones were analyzed by Southern blotting using EcoRI and an external ~500 bp probe. Correctly targeted ES cells were injected into C57BL/6 blastocysts to generate chimeras that were backcrossed with strains C57BL/6, SvJ, or NMRI. Heterozygous offspring were crossed to yield homozygous mutant animals. The present studies were performed with the F2 and F3 generations. Two independent embryonic stem cell clones gave $Kcc2^{-/-}$ mice whose phenotypes were indistinguishable. The phenotype of $Kcc2^{-/-}$ animals did not depend on the genetic backgrounds used.

In Situ Hybridization

Antisense RNA probes labeled with (α-^{35}S)-UTP were generated with T7 polymerase from linearized cDNA subclones according to the manufacturer's instructions (Ambion). Probes were resuspended in hybridization mix containing 50% formamide, 1 × Denhardt's solution, 4 × SSC, 5% dextran sulfate, 500 μg/ml yeast tRNA, and 10 mM DTT to a minimum of 2×10^6 cpm/ml. Ten micrometer cryosections were fixed in 4% paraformaldehyde (PFA) in phosphate buffered saline (PBS), acetylated, dehydrated, and subjected to in situ hybridization at 55°C for 18 hr. The slides were washed with 4 × SSC and subsequently treated with RNase A (10 mM Tris-HCl, pH 8.0, 500 mM NaCl, 1 mM EDTA, 20 μg/ml RNase A) for 30 min at 37°C. The slides were then washed and desalted. A 30 min high-stringency wash was performed in 0.1 × SSC at 55°C. Sections were dehydrated and exposed to high resolution X-ray films (Kodak Biomax MR). Subsequently, the slides were dipped into Kodak NTB-2 nuclear track emulsion, developed after 3 to 6 weeks in Kodak Dektol, and stained with Giemsa (Sigma). Specificity of the signals was verified by comparing antisense with sense controls. Probes comprised nucleotides 159 to 697 for KCC1 (corresponding to amino acids 53 to 232), nucleotides 59 to 557 for KCC2 (amino acids 63 to 229), nucleotides 2060 to 2620 for KCC3 (amino acids 653 to 839), nucleotides 615 to 1206 for NKCC1 (amino acids 163 to 360), and nucleotides 259 to 903 for ClC-2 (amino acids 67 to 281) of the mouse cDNA.

RNA Isolation, Northern Blot

Total RNA was obtained from pooled E18.5 spinal cord preparations of $Kcc2^{-/-}$ and WT animals, respectively, by extraction with Trizol (Life Technologies). Poly(A)$^+$ RNA was purified with Dynabeads Oligo(dT)$_{25}$ (DYNAL), separated by electrophoresis, and blotted following standard protocols. Hybridization was performed with an end-labeled 49 b oligonucleotide spanning exon 5 using standard procedures.

RNase Protection Assay

RNA of pooled E18.5 spinal cords of each genotype was prepared as described above. Three independent RNase protection experiments were performed. (α-^{32}P)-UTP labeled antisense probes were transcribed from the same templates as for in situ hybridization. The KCC4 probe comprised nucleotides 144 to 531 of the mouse cDNA (corresponding to amino acids 25 to 153). Prior to use, probes were purified by denaturing gel electrophoresis and subsequent elution of the appropriate transcript. Ten micrograms RNA each were subjected to ribonuclease protection assays, which used the HybSpeed RPA kit (Ambion) according to the manufacturer's instructions. RNA was simultaneously hybridized with a 300 bp fragment β-actin probe providing a normalizing reference for further analysis. After RNase digestion, the precipitated fragments were separated on a 5% sequencing gel and analyzed by autoradiography and scanning.

Western Blot

The KCC2 antiserum was raised in rabbits against the amino-terminal epitope CEDGDGGANPGDGNP coupled to BSA through the C-terminal cysteine and affinity purified. It was highly specific, as no signals were detected in $Kcc2^{-/-}$ mice by Western analysis or immunofluorescence. Western blots of lysates of brain and spinal cord tissue (20 μg per lane) were probed with rabbit antiserum (1:500)

or rabbit anti-actin (Sigma) (1:2000) as a loading control. Detection used a chemiluminescence kit (Renaissance, DuPont).

Immunofluorescence

For immunofluorescence, spinal cord preparations of E18.5 or adult animals were fixed in 4% PFA in PBS, embedded in 2% agarose, and cut into 50 μm slices with a vibratome (Leica). Slices were incubated in 10%, 20%, 40%, 20%, 10% ethanol for 10 min each and subsequently blocked with 10% serum and 0.2% BSA in PBS for 30 min. Incubation of primary antibodies was done in carrier (PBS with 1% serum and 0.2% BSA) at 4°C overnight. Gephyrin staining was performed after incubation of slices for 10 min in PBS including 50 mM ammonium chloride. Primary antibodies were from Roche (MAP2), the Developmental Studies Hybridoma Bank (Iowa) (NF), and from Alexis (gephyrin). Slices were washed three times with PBS and incubated with the secondary antibodies. Secondary antibodies were the Alexa Fluor 546 coupled goat anti-rabbit and Alexa Fluor 488 coupled goat anti-mouse (Molecular Probes). After three final washes, slices were mounted with Fluoromount (EMS). Analysis was done by confocal microscopy (Leica TCS).

Electron Microscopy

For electron microscopy, adult spinal cords were fixed in 4% PFA in PBS with 1% glutaraldehyde. Fifty micrometer sections were blocked with 5% normal goat serum, 0.5% BSA, and 0.1% gelatine in PBS. Sections were incubated with KCC2 antiserum in 0.1% gelatine and 0.5% BSA in PBS and subsequently with goat anti-rabbit nano gold (Biotrend). The signal was enhanced with the IntensEM kit (Biorad). Slices were finally treated with 1% Osmium on ice, dehydrated in an ascending series of ethanol, and embedded in Epon (Roth). Ultrathin sections (60 nm) were examined with a Zeiss EM 902.

Extracellular Nerve Recordings

Respiratory activity was monitored from cervical ventral rootlets of isolated brainstem preparations of E18.5 mice. They were prepared as described (Onimaru and Homma, 1987; Suzue, 1984) and continuously superfused at 30°C with 95% O_2/5% CO_2 gassed artificial cerebrospinal fluid (ASCF) that contained (mM) 118 NaCl, 1 NaH$_2$PO$_4$, 25 NaHCO$_3$, 3 KCl, 1 MgCl$_2$, and 1.5 CaCl$_2$. Signals were amplified by a custom made differential amplifier, filtered, and subsequently rectified and integrated. For sciatic nerve recordings, E18.5 animals were decapitated, eviscerated, and immediately transferred into gassed ACSF. A ventral laminectomy exposed the dorsal surface of the spinal cord. The sciatic nerve was carefully dissected to keep its connection with the spinal cord intact. Sharp microelectrodes filled with 3 M KCl were impaled into the nerve. Signals were amplified by a differential amplifier. Stimuli were generated by a pulse stimulator (A-M System). Pulse duration was 200 μs. The threshold amplitude was approximately 10 V.

Patch-Clamp Studies

Spinal cord preparations were obtained essentially as described above and were then embedded in 1% agarose. The lumbar spinal cord was sliced horizontally (350 μm) with a vibratome (Leica). Slices were continuously superfused with gassed ACSF. Motoneurons were identified with DIC-infrared video microscopy by their location in the ventral horns and the large diameter of their somata (>20 μm). Electrodes (3–5 MΩ) were made from thick-wall borosilicate glass (Clark Electromedical). Pipette solution contained (mM) 140 KCl, 2 MgCl$_2$, 10 Hepes, 5 EGTA at pH 7.4. Gramicidin (Sigma) concentration was 1–5 μg/ml. Membrane potentials were measured with an Axopatch 200A (Axon) in the current-clamp (I = 0) or voltage-clamp mode. The voltage clamp protocol consisted of stepping the membrane from a holding potential of -60 to $+20$ mV for 80 ms, then changing the voltage to -100 mV at a rate of 150 mV/s. Recordings and analysis were done with pClamp 8.0 (Axon).

References

Ballanyi, K., Onimaru, H., and Homma, I. (1999). Respiratory network function in the isolated brainstem-spinal cord of newborn rats. Prog. Neurobiol. *59*, 583–634.

Ben-Ari, Y., Khazipov, R., Leinekugel, X., Caillard, O., and Gaiarsa, J.L. (1997). GABA$_A$, NMDA and AMPA receptors: a developmentally regulated 'menage à trois'. Trends Neurosci. *20*, 523–529.

Biscoe, T.J., and Duchen, M.R. (1986). Synaptic physiology of spinal motoneurones of normal and spastic mice: an in vitro study. J. Physiol. A (Lond.) *379*, 275–292.

Bösl, M.R., Stein, V., Hübner, C., Zdebik, A.A., Jordt, S.E., Mukhopadhyay, A.K., Davidoff, M.S., Holstein, A.F., and Jentsch, T.J. (2001). Male germ cells and photoreceptors, both dependent on close cell-cell interactions, degenerate upon ClC-2 Cl-channel disruption. EMBO J. *20*, 1289–1299.

Buckle, P.J., and Spence, I. (1981). A simple in vivo method for evaluating drug action at central and peripheral synapses. Naunyn Schmiedebergs Arch. Pharmacol. *315*, 211–218.

Cherubini, E., Gaiarsa, J.L., and Ben-Ari, Y. (1991). GABA: an excitatory transmitter in early postnatal life. Trends Neurosci. *14*, 515–519.

Clayton, G.H., Owens, G.C., Wolff, J.S., and Smith, R.L. (1998). Ontogeny of cation-Cl-cotransporter expression in rat neocortex. Brain Res. Dev. Brain Res. *109*, 281–292.

Delpire, E., Lu, J., England, R., Dull, C., and Thorne, T. (1999). Deafness and imbalance associated with inactivation of the secretory Na-K-2Cl co-transporter. Nat. Genet. *22*, 192–195.

Feldman, J.L., and Smith, J.C. (1989). Cellular mechanisms underlying modulation of breathing pattern in mammals. Ann. NY Acad. Sci. *563*, 114–130.

Flint, A.C., Liu, X., and Kriegstein, A.R. (1998). Nonsynaptic glycine receptor activation during early neocortical development. Neuron *20*, 43–53.

Gao, B.X., and Ziskind-Conhaim, L. (1995). Development of glycine- and GABA-gated currents in rat spinal motoneurons. J. Neurophysiol. *74*, 113–121.

Gillen, C.M., Brill, S., Payne, J.A., and Forbush, B., 3rd (1996). Molecular cloning and functional expression of the K-Cl cotransporter from rabbit, rat, and human. A new member of the cation-chloride cotransporter family. J. Biol. Chem. *271*, 16237–16244.

Goodman, C.S., and Shatz, C.J. (1993). Developmental mechanisms that generate precise patterns of neuronal connectivity. Cell Suppl. *72*, 77–98. [Neuron Suppl. *10*, 77–98.]

Haas, M., and Forbush, B., 3rd (1998). The Na-K-Cl cotransporters. J. Bioenerg. Biomembr. *30*, 161–172.

Kirsch, J., and Betz, H. (1995). The postsynaptic localization of the glycine receptor-associated protein gephyrin is regulated by the cytoskeleton. J. Neurosci. *15*, 4148–4156.

Kneussel, M., and Betz, H. (2000). Receptors, gephyrin and gephyrin-associated proteins: novel insights into the assembly of inhibitory postsynaptic membrane specializations. J. Physiol. A (Lond.) *525*, 1–9.

Kyrozis, A., and Reichling, D.B. (1995). Perforated-patch recording with gramicidin avoids artifactual changes in intracellular chloride concentration. J. Neurosci. Methods *57*, 27–35.

Lloyd, D.P.C. (1943). Conduction and synaptic transmission of reflex response to stretch in spinal cats. J. Neurophysiol. *6*, 317–326.

LoTurco, J.J., Owens, D.F., Heath, M.J., Davis, M.B., and Kriegstein, A.R. (1995). GABA and glutamate depolarize cortical progenitor cells and inhibit DNA synthesis. Neuron *15*, 1287–1298.

Mount, D.B., Mercado, A., Song, L., Xu, J., George, A.L., Jr., Delpire, E., and Gamba, G. (1999). Cloning and characterization of KCC3

and KCC4, new members of the cation-chloride cotransporter gene family. J. Biol. Chem. *274*, 16355–16362.

Obrietan, K., and van den Pol, A.N. (1997). GABA activity mediating cytosolic Ca^{2+} rises in developing neurons is modulated by cAMP-dependent signal transduction. J. Neurosci. *17*, 4785–4799.

Onimaru, H., and Homma, I. (1987). Respiratory rhythm generator neurons in medulla of brainstem-spinal cord preparation from newborn rat. Brain Res. *403*, 380–384.

Pace, A.J., Lee, E., Athirakul, K., Coffman, T.M., O'Brien, D.A., and Koller, B.H. (2000). Failure of spermatogenesis in mouse lines deficient in the Na$^+$-K$^+$-2Cl$^-$ cotransporter. J. Clin. Invest. *105*, 441–450.

Payne, J.A., Stevenson, T.J., and Donaldson, L.F. (1996). Molecular characterization of a putative K-Cl cotransporter in rat brain. A neuronal-specific isoform. J. Biol. Chem. *271*, 16245–16252.

Prichard, J.W., Gallagher, B.B., and Glaser, G.H. (1969). Experimental seizure-threshold testing with fluorthyl. J. Pharmacol. Exp. Ther. *166*, 170–178.

Randall, J., Thorne, T., and Delpire, E. (1997). Partial cloning and characterization of Slc12a2: the gene encoding the secretory Na$^+$-K$^+$-2Cl$^-$ cotransporter. Am. J. Physiol. *273*, C1267–C1277.

Rivera, C., Voipio, J., Payne, J.A., Ruusuvuori, E., Lahtinen, H., Lamsa, K., Pirvola, U., Saarma, M., and Kaila, K. (1999). The K$^+$/Cl$^-$ co-transporter KCC2 renders GABA hyperpolarizing during neuronal maturation. Nature *397*, 251–255.

Schneider, S.P., and Fyffe, R.E. (1992). Involvement of GABA and glycine in recurrent inhibition of spinal motoneurons. J. Neurophysiol. *68*, 397–406.

Simon, D.B., Karet, F.E., Hamdan, J.M., DiPietro, A., Sanjad, S.A., and Lifton, R.P. (1996a). Bartter's syndrome, hypokalaemic alkalosis with hypercalciuria, is caused by mutations in the Na-K-2Cl cotransporter NKCC2. Nat. Genet. *13*, 183–188.

Simon, D.B., Nelson-Williams, C., Bia, M.J., Ellison, D., Karet, F.E., Molina, A.M., Vaara, I., Iwata, F., Cushner, H.M., Koolen, M., et al. (1996b). Gitelman's variant of Bartter's syndrome, inherited hypokalaemic alkalosis, is caused by mutations in the thiazide-sensitive Na-Cl cotransporter. Nat. Genet. *12*, 24–30.

Smith, J.C., Ellenberger, H.H., Ballanyi, K., Richter, D.W., and Feldman, J.L. (1991). Pre-Botzinger complex: a brainstem region that may generate respiratory rhythm in mammals. Science *254*, 726–729.

Smith, R.L., Clayton, G.H., Wilcox, C.L., Escudero, K.W., and Staley, K.J. (1995). Differential expression of an inwardly rectifying chloride conductance in rat brain neurons: a potential mechanism for cell-specific modulation of postsynaptic inhibition. J. Neurosci. *15*, 4057–4067.

Staley, K., Smith, R., Schaack, J., Wilcox, C., and Jentsch, T.J. (1996). Alteration of GABA$_A$ receptor function following gene transfer of the CLC-2 chloride channel. Neuron *17*, 543–551.

Sun, D., and Murali, S.G. (1999). Na$^+$-K$^+$-2Cl$^-$ cotransporter in immature cortical neurons: A role in intracellular Cl-regulation. J. Neurophysiol. *81*, 1939–1948.

Sung, K.W., Kirby, M., McDonald, M.P., Lovinger, D.M., and Delpire, E. (2000). Abnormal GABA$_A$ receptor-mediated currents in dorsal root ganglion neurons isolated from Na-K-2Cl cotransporter null mice. J. Neurosci. *20*, 7531–7538.

Suzue, T. (1984). Respiratory rhythm generation in the in vitro brain stem-spinal cord preparation of the neonatal rat. J. Physiol. A (Lond.) *354*, 173–183.

Thiemann, A., Grunder, S., Pusch, M., and Jentsch, T.J. (1992). A chloride channel widely expressed in epithelial and non-epithelial cells. Nature *356*, 57–60.

Vardi, N., Zhang, L.L., Payne, J.A., and Sterling, P. (2000). Evidence that different cation chloride cotransporters in retinal neurons allow opposite responses to GABA. J. Neurosci. *20*, 7657–7663.

Voipio, J., and Kaila, K. (2000). GABAergic excitation and K$^+$-mediated volume transmission in the hippocampus, Vol. 125 (Amsterdam: Elsevier Science).

Vu, T.Q., Payne, J.A., and Copenhagen, D.R. (2000). Localization

and developmental expression patterns of the neuronal K-Cl cotransporter (KCC2) in the rat retina. J. Neurosci. *20*, 1414–1423.

Wentworth, L.E. (1984). The development of the cervical spinal cord of the mouse embryo. I. A Golgi analysis of ventral root neuron differentiation. J. Comp. Neurol. *222*, 81–95.

Williams, J.R., Sharp, J.W., Kumari, V.G., Wilson, M., and Payne, J.A. (1999). The neuron-specific K-Cl cotransporter, KCC2. Antibody development and initial characterization of the protein. J. Biol. Chem. *274*, 12656–12664.

Yuste, R., and Katz, L.C. (1991). Control of postsynaptic Ca^{2+} influx in developing neocortex by excitatory and inhibitory neurotransmitters. Neuron *6*, 333–344.

Zhang, S.J., and Jackson, M.B. (1993). GABA-activated chloride channels in secretory nerve endings. Science *259*, 531–534.